ACS APPLIED MATERIALS & INTERFACES

Letter

www.acsami.org

Ultrafast Nanofiltration through Large-Area Single-Layered Graphene Membranes

Yanzhe Qin,[†,‡] Yongyou Hu,[*,†] Stephan Koehler,[‡] Liheng Cai,[‡] Junjie Wen,[†] Xiaojun Tan,[†] Weiwei L. Xu,[§] Qian Sheng,[∥] Xu Hou,[⊥] Jianming Xue,[∥] Miao Yu,[*,§] and David Weitz[†]

[†]The Key Lab of Pollution Control and Ecosystem Restoration in Industry Clusters, Ministry of Education, School of Environment and Energy, South China University of Technology, Guangzhou Higher Education Mega Centre, Guangzhou 510006, China

[‡]John A. Paulson School of Engineering and Applied Sciences, Harvard University, 29 Oxford Street, Cambridge, Massachusetts 02138, United States

[§]Department of Chemical Engineering, Catalysis for Renewable Fuels Center, University of South Carolina, Columbia, South Carolina 29208, United States

[∥]State Key Lab of Nuclear Physics and Technology, Beijing University, Beijing 100871, China

[⊥]Collaborative Innovation Center of Chemistry for Energy Materials, College of Chemistry and Chemical Engineering, Xiamen University, Xiamen 361005, China

Supporting Information

ABSTRACT: Perforated single-layered graphene has demonstrated selectivity and flux that is orders of magnitude greater than state-of-the-art polymer membranes. However, only individual graphene sheets with sizes up to tens of micrometers have been successfully fabricated for pressurized permeation studies. Scaling-up and reinforcement of these atomic membranes with minimum cracks and pinholes remains a major hurdle for practical applications. We develop a large-area in situ, phase-inversion casting technique to create 63 cm^2 high-quality single-layered perforated graphene membranes for ultrafast nanofiltration that can operate at pressures up to 50 bar. This result demonstrates the feasibility of our technique for creating robust large-area, high quality, single-layered graphene and its potential use as a pressurized nanofiltration membrane.

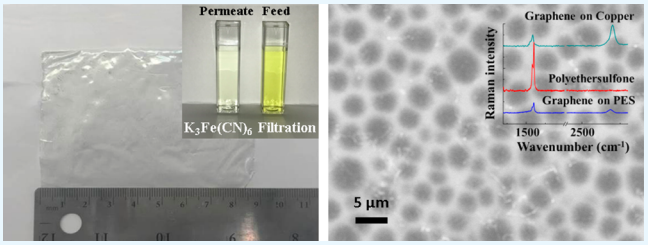

KEYWORDS: *graphene transfer, high-quality graphene, large area graphene, graphene nanofiltration, phase inversion, molecular sieving, nanoporous graphene*

Monolayer graphene, a sp^2-bonded allotrope of carbon arranged in a two-dimensional lattice, exhibits extraordinary imperviousness and mechanical properties in its pristine form, making it an ideal material for membrane applications.[1−3] Recent proof-of-principle experiments have shown that the performance of graphene in certain applications, such as ultrafast gas/liquid separation,[4−6] highly sensitive sensing,[7−9] and high-throughput DNA sequencing,[10] far exceeds the state-of-the-art. In these applications, high quality graphene has to be suspended, which due to limitations of current fabrication techniques restricts the accessible size to tens of microns. Most attempts to support the graphene sheets are based upon introducing pores in the substrate onto which the graphene has been deposited or transferred, such as masking of photoresist and etching of copper.[10,11] Both the complexity of this process and its lacking reliability for creating large-area graphene membranes prevents mass-production. Other attempts to fabricate large area suspended graphene membranes have been based on adhering CVD grown graphene sheets onto prefabricated porous supporting layers.[12−14] However, in addition to inevitable lattice defects occurring during CVD growth, the transfer process introduces further defects, such as pinholes or cracks that are due to microscopic mismatches between the graphene and the supporting substrate. Although these defects can be sealed, they still are prone to failure in pressurized membrane applications such as filtration.[13] Robust techniques for fabrication of large-area high-quality suspended graphene sheets are still lacking, which prevents their commercialization for practical applications that are based on 2D membranes.[15,16]

We have developed a facile and robust liquid-casting fabrication technique for seamlessly transferring large-area, single-layered graphene with a minimum of nonselective defects onto porous polymer substrate. The workflow is shown in Figure 1a. We purchase a high-quality chemical vapor deposition (CVD) single-layered graphene sheet on a flat copper substrate, coat the exposed graphene surface with solution of 10%−20% poly(ether sulfone) (PES) in *N*-methyl-

Received: January 11, 2017
Accepted: March 9, 2017
Published: March 9, 2017

DOI: 10.1021/acsami.7b00504
ACS Appl. Mater. Interfaces 2017, 9, 9239−9244

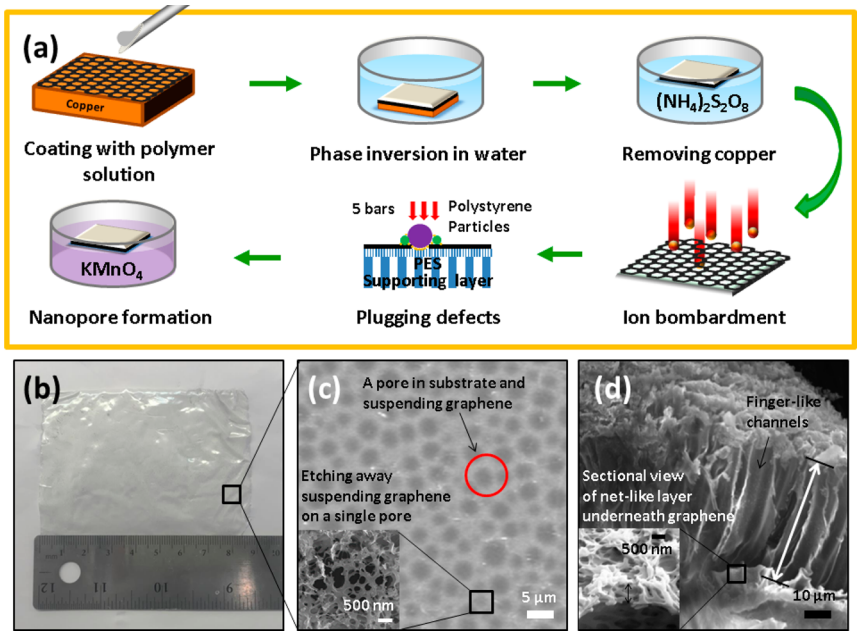

Figure 1. Fabrication and characterization of crack-free graphene composite membrane. (a) Schematic of the fabrication process. Step 1: uniformly coat the CVD graphene on copper with a polymer solution. Step 2: immerse the coated structure in water causing phase inversion whereby a porous network is formed. Step 3: remove of copper by floating the structure on a persulfate ammonia solution. Step 4: gallium ion bombardment introduces nonporous lattice defects in the graphene. Step 5: seal defects by filtration of polystyrene nanoparticles at 5 bar followed by drying. Step 6: etch in acidic potassium permanganate to enlarge defects into nanopores. (b) Photograph (top view) of a 9 CM x 7 CM final graphene composite membrane. Note that the pressurized side can only be the graphene side. (c) SEM image shows the integrity of the graphene composite membrane (scale bar is 5 μm). Inset shows the netlike structure of the PES substrate after the graphene has been etched away (scale bar is 500 nm). (d) Cross-section SEM image of the composite graphene membrane reveals long fingerlike pores that span the membrane (scale bar is 10 μm). Inset is a close up of the netlike structure directly underneath the graphene (scale bar is 500 nm).

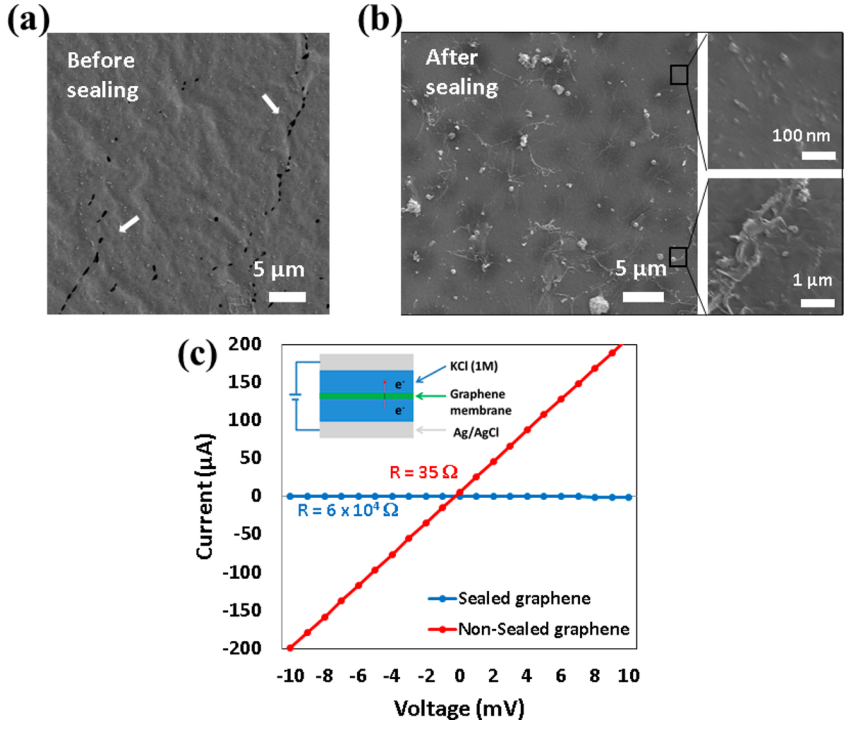

Figure 2. Defect sealing of graphene composite membrane. (a) SEM image of the graphene before sealing reveals hole defects that are less than 300 nm; defects are shown by arrows. (b) SEM image of the graphene after sealing process shows nanoparticle deposits that clog the hole defects. (c) Ionic conductance measurements of the for a 5 × 5 mm graphene membrane before and after defect sealing. The electrical resistance before sealing is 35 Ω, which increases by 3 orders of magnitude to 6 × 10^4 Ω after sealing. The upper left inset is a schematic of the experimental setup.

2-pyrrolidone (NMP), and subsequently immerse it in water (see method). The NMP solvent diffuses into water leaving behind an ~100 μm thick solid conformal porous membrane that is strongly adherent to graphene, in a process known as

DOI: 10.1021/acsami.7b00504
ACS Appl. Mater. Interfaces 2017, 9, 9239−9244

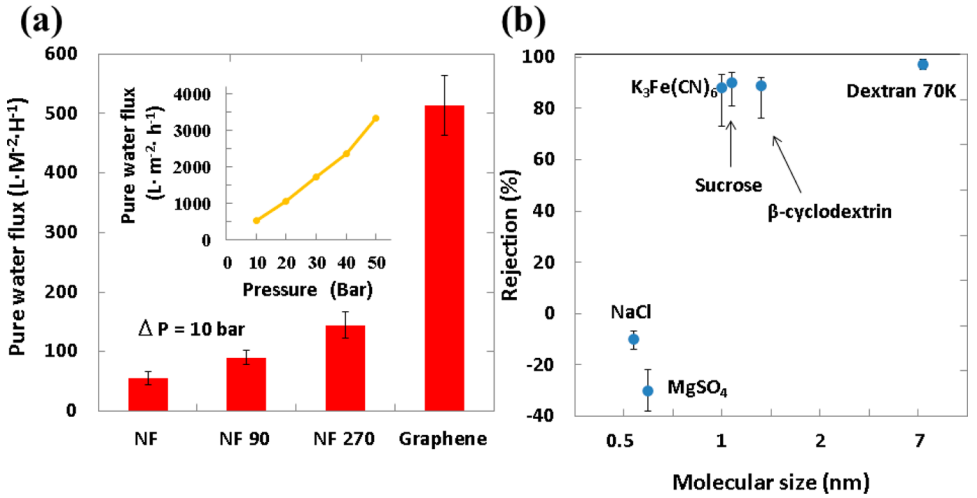

Figure 3. Selectivity and flux performance of graphene composite membrane. (a) Comparison of pure water flux for three commercial Dow membrane (MWCO 200−400 Da, see manufacturer's datasheet for rejection) NF, NF90, and NF270 with our graphene membrane at 10 bar of applied pressure. Inset shows the relationship between pure water flux and pressure for our membrane. (b) Rejection of six standard molecules at 10 bar. The reported size for the three ions $K_3Fe(CN)_6$, NaCl, and $MgSO_4$ is the hydrated diameter, and for three molecules (dextran 70K, β-cyclodextrin, and sucrose) is the molecular diameter.

phase inversion (Figure S1).[17] We then dissolve the copper substrate in persulfate ammonia and wash the composite membrane in water and methanol. The exposed graphene surface is bombarded by a low energy Ga^+ ion beam that creates high-density, water-impermeable defect nucleation centers.[18] To seal the inevitable very low density pinholes and cracks, we filter an aqueous suspension of impermeable polystyrene nanoparticles, which plug these defects and adhere to the underlying PES layer. We then perform an acidic potassium permanganate etch to open up the defect nucleation centers and create atomic-scale pores with density of $\sim 1.57 \times 10^{12}$ water permeable pores per cm^2.[13]

The phase inversion transfer method is highly reliable, and resulting membrane is mechanically stable and easy to handle without extreme precautions. Visual inspection shows a smooth surface, and the graphene sheet appears to completely cover the polymeric substrate, see Figure 1b and method. SEM images show an almost complete covering of graphene on the porous substrate without tears or cracks, see Figure 1c and Figure S2a, b; however, a very small fraction of the area (<0.003% from the SEM images analyzed by image J) has hole defects (<300 nm) usually arranged in linear or cluster patterns, as shown by the arrows in Figure 2a. These defects are consistent with those observed from other high-quality CVD-graphene transfer processes, and most likely occur during the CVD growth.[19] Filtration of pure water shows negligible flux, which demonstrates high quality of graphene and limited contribution of flux thorough lattice defects occurring during CVD growth and low density of large defects; filtration of aqueous $K_3Fe(CN)_6$ solution shows no obvious rejection, which demonstrates the large defects are nonselective and the necessity of defect sealing, as discussed below. We use Raman spectroscopy to detect atomic defects associated with the D-band (1350 cm^{-1}), and the absence of the 1350 cm^{-1} peak indicates the defect density is less than one per μm^2, see Figure S2c.[20]

The in situ casted PES polymer substrate is well-suited for supporting the graphene sheet at high pressure while providing little flow resistance.[21] Previous work has shown that elongated macrovoids form when PES/NMP polymer solvent pair is coagulated in water (see method).[22] The structural support and pore geometry depends on the casting solution, and for our purposes we cast a PES layer with a void fraction of 35%. This substrate has three types of porous structures as can be seen in Figure 1c, d. Attached directly underneath the graphene sheet is an ultrathin (~500 nm) netlike layer that binds very strongly to honeycomb lattice carbon, as shown in the control experiment using graphite (see discussion in Figure S3). It has through holes of 50−500 nm in diameter as shown in the close ups of Figure 1c, d. The second structure is fingerlike pores that are channels extending from the net-like layer to the bottom of the substrate, as shown in Figure 1d, which have an average pore size of 3 μm and pore density of $4.5 \times 10^6/cm^2$ as shown in Figure S2d. The very bottom of the substrate is a microporous layer that has negligible transport resistance to water for the current transferred graphene membrane, and can be removed upon further development of high water flux graphene membrane, as discussed below.

We next characterize the graphene membrane before performing the final etching step that results in ~1 nm pores. At this point, the graphene sheet has been bombarded by ions but defect nucleation centers have not yet been opened by etching (see discussion below), but both pinholes and cracks that account for very small portion of total area have been sealed by filtering an aqueous suspension of polystyrene particles ranging in size from 30 nm to 2 μm, using the setup shown in Figure S4a. These particles are entrained by the flow and form deposits that adhere to the PES net-like structure directly beneath the defects and thereby seal the defects, as shown in Figure 2b. The particles adhere sufficiently strongly such that a surface flow by vigorous stirring cannot unseat them. Also, sealed membrane can withstand up to 50 bar of hydrostatic pressure without breakage, and even at this high pressure, we cannot collect any permeate in dead-end filtration, suggesting sealing by polystyrene particles is effective and the remaining defects are minimal (setup as shown in Figure S4b). In addition, we perform ionic measurement in solution across the graphene membrane, which is highly sensitive to existence of nanopores (setup as shown in Figure S4c). After sealing, the average electrical resistance coefficient K is 1250 kΩ mm^2 (K =

DOI: 10.1021/acsami.7b00504
ACS Appl. Mater. Interfaces 2017, 9, 9239−9244

resistance × area), which is 1000 times greater than that before sealing and 5 times higher than that of a 5 × 5 μm graphene sheet reported to exhibit desalination filtration,[6] see Figure 2c. This result further suggests this method effectively seal the pinholes and cracks.[10]

Next, we quantify the pure water flux of our graphene membrane after etching. As previously reported, the etching process opens up the nucleation centers and forms water permeable pores, which is a high initial barrier reaction.[23] The duration of the acidic potassium permanganate etching dictates the rejection and the flux; after 5 min of etching, we still cannot collect permeate even after several hours' pressurization. Longer etching increases the water flux, which exceeds 4000 L M^{-2} H^{-1} at 10 bar pressure drop after several hours. After appropriate etching time optimization, the highest water flux we obtained is exceeding 500 L M^{-2} H^{-1} at 10 bar pressure drop (Figure 3a), while maintaining high rejection for organic molecules smaller than 1 nm (see discussion below). Noted that methanol is used to wet the back side of graphene membrane before testing to increase its flux. To test our membrane's stability, we apply a range of higher pressures, 10−50 bar and observe an approximately linear dependence of the water flux, as shown in the inset of Figure 3a. After high pressure filtration of pure water for 3 h, the membrane remains intact and its permeance at low pressures remains unchanged, as shown in Figure S5. This result indicates the phase inversion technique creating a PES supporting layer with appropriate pore structure that is able to support suspend graphene at high pressure, which is in consistence with earlier simulation.[21] At 25 °C and 10 bar, compared with the state-of-the-art polymeric nanofiltration membrane, the pure flux of our membrane is 5−10 times greater in dead-end filtration. After removal of the dense bottom PES layer, the water flux did not show apparent increase, suggesting the main mass transfer resistance is within the graphene layer, see Figure S6. We hypothesize the relatively low water flux through the single-layered graphene membrane might be due to low conversion ratio (4%) of the defect nucleation centers into water permeable pores during the etching step. As previously reported, most of the nanopores are smaller than the water molecule, and thus the available water permeation area of the graphene membrane is only about 1% of the total area.[13]

We test the rejection of our graphene membrane for a range of molecular sizes varying from 0.5 to 7 nm at pressure of 10 bar. For molecules with hydrated radius exceeding 0.9 nm but smaller than 7 nm, such as $K_3Fe(CN)_6$, sucrose, β-cyclodextrin, we observe an average rejection of approximately 90%, and for Dextran 70000 (7 nm), rejection as high as 98% is seen, as shown in Figure 3b. This result suggests a narrow distribution of pore sizes, and the molecular weight cutoff (MWCO) is below 329 Da ($K_3Fe(CN)_6$), ∼0.9 nm. Because a small fraction of these larger molecules does pass through the filter, we speculate that our graphene composite membrane does have a small fraction of pores or unsealed defects with a size smaller than that of dextran 70K (∼7 nm) but larger than that of $K_3Fe(CN)_6$ (∼0.9 nm). In 2 h filtration tests of pure water, oil, and aqueous solutions containing organic molecules ($K_3Fe(CN)_6$, sucrose, β-cyclodextrin), we observe no or only slight flux decrease at 10 bar. Smaller molecules with a hydrated radius <0.9 nm, such as $MgSO_4$ and NaCl, we observe enrichment rather than rejection. This indicates the pores we created are larger than the hydrated diameters of these smaller ions, and we attribute their fast passage through the pores to charge interactions with the graphene pores, which is observed in previous graphene permeation studies.[24]

To address the important issue of biofilm fouling, which is one of the major failure modes in aqueous environments, we expose our graphene membrane to a 1 × 10^7 CFU/mL suspension of *E. coli* for 5 h.[25] We dissociate bacteria from the membrane surface and recultivate the suspension on agar. On average we observe no colonies, which indicates that bacteria cannot successfully adhere to the membrane, as shown in Figure 4a. As a control we repeat this experiment for Dow NF 270 which is a comparable commercial polymeric nanofiltration membrane, and observe numerous colonies as shown in Figure 4b. Additionally we take SEM images of both membranes after 24 h exposure to the bacterial suspension after the surface is gently washed with pure water. The graphene membrane shows no adhered bacteria, whereas for the polymer membrane bacteria adheres to the surface, as shown in Figure 4c, d, respectively. The low bonding affinity to *E. coli* of graphene membrane indicates potential less bactericide usage and decreased biosourced membrane failure.

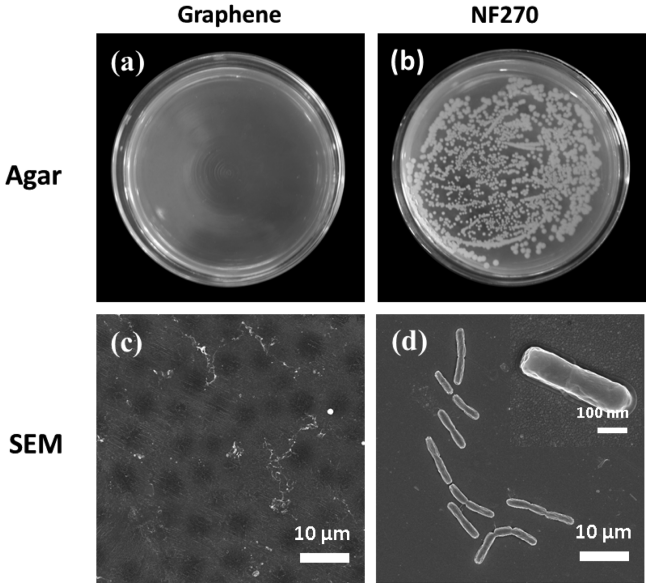

Figure 4. Bacteria do not attach to graphene composite membrane. Photographs of culture plates showing *E. coli* colonies grown from the bacterial suspensions dissociated from the (a) graphene and (b) Dow NF 270 polymeric membrane surfaces. SEM images of the (c) graphene and (d) polymer membranes after exposure to a bacterial suspension for 24 h.

In conclusion, we demonstrate a facile and robust fabrication technique to transfer high-quality, large-area single-layered graphene onto porous substrates that can withstand high pressures up to at least 50 bar. Because our technique is based on liquid casting, it is expected to be compatible with current roll-to-roll mass-production processes.[26,27] Further, we demonstrate the potential of our membrane for nanofiltration by perforation through Ga^+ bombardment followed by etching. The pure water flux is 500 L M^{-2} H^{-1} at 10 bar, which is at least five times greater than state-of-the-art polymer membranes with similar molecular weight cut-offs. Our membrane is highly resistant to biofouling, which in practical uses may significantly prolong membrane service time and lower maintenance cost. Moreover, the low/competing binding affinity and 2D morphology of the graphene separation layer is beneficial for

DOI: 10.1021/acsami.7b00504
ACS Appl. Mater. Interfaces 2017, 9, 9239−9244

biomedical separation applications involving extremely low concentration or low volume feeds, which cannot be realized by conventional polymeric membranes because of their adsorption/retention in the 3D porous separation layer.[28] Future improvements in graphene perforation methods to make higher density, smaller and more uniform pores should improve performance and enable energy-efficient water desalination and gas separation.[29,30] The high quality and scalability of the single-layered graphene membrane fabrication technique make graphene separation membrane feasible and is an attractive option for nanofiltration of small molecules.

■ ASSOCIATED CONTENT

Supporting Information

The Supporting Information is available free of charge on the ACS Publications website at DOI: 10.1021/acsami.7b00504.

Figures S1−S6 (PDF)

■ AUTHOR INFORMATION

Corresponding Authors

*E-mail: ppyyhu@scut.edu.cn.
*E-mail: yumiao@cec.sc.edu.

ORCID

Yanzhe Qin: 0000-0001-9414-028X
David Weitz: 0000-0001-6678-5208

Author Contributions

Y.Q. designed, characterized, and tested the composite graphene membrane. J.X. and Q.S. conducted sample ion bombardment by 2 × 1.7 MV tandem. J.W. carried out the antibiofouling experiments. W.X. performed gas permeation measurements. L.C. provided key suggestiosn to crack-free membrane fabrication. S.K. helped with writing. M.Y. provided suggestions for membrane pore size characterization and permeation measurements. All authors discussed, interpreted data, and wrote the paper.

Notes

The authors declare no competing financial interest.

■ ACKNOWLEDGMENTS

We thank A. Kuan for suggestions and help on building electrical resistance measurement setup; J. Park for discussion on figures; and X. Lou for assistance with sample bombardment by FIB. We thank the Chinese Scholarship Council. This work is supported by the National Science Foundation (NSF; award No. CBET-1451887), the Harvard Materials Research Science and Engineering Center.

■ REFERENCES

(1) Frank, I. W.; Tanenbaum, D. M.; Van der Zande, A. M.; McEuen, P. L. Mechanical Properties of Suspended Graphene Sheets. *J. Vac. Sci. Technol. B* **2007**, *25*, 2558−2561.

(2) Bunch, J. S.; Verbridge, S. S.; Alden, J. S.; van der Zande, A. M.; Parpia, J. M.; Craighead, H. G.; McEuen, P. L. Impermeable Atomic Membranes from Graphene Sheets. *Nano Lett.* **2008**, *8*, 2458−2462.

(3) Berry, V. Impermeability of Graphene and its Applications. *Carbon* **2013**, *62*, 1−10.

(4) Celebi, K.; Buchheim, J.; Wyss, R. M.; Droudian, A.; Gasser, P.; Shorubalko, I.; Kye, J. I.; Lee, C.; Park, H. G. Ultimate Permeation across Atomically Thin Porous Graphene. *Science* **2014**, *344*, 289−292.

(5) Koenig, S. P.; Wang, L.; Pellegrino, J.; Bunch, J. S. Selective Molecular Sieving through Porous Graphene. *Nat. Nanotechnol.* **2012**, *7*, 728−732.

(6) Surwade, S. P.; Smirnov, S. N.; Vlassiouk, I. V.; Unocic, R. R.; Veith, G. M.; Dai, S.; Mahurin, S. M. Water Desalination using Nanoporous Single-layer Graphene. *Nat. Nanotechnol.* **2015**, *10*, 459−464.

(7) Cheng, Z.; Li, Q.; Li, Z.; Zhou, Q.; Fang, Y. Suspended Graphene Sensors with Improved Signal and Reduced Noise. *Nano Lett.* **2010**, *10*, 1864−1868.

(8) Smith, A. D.; Niklaus, F.; Paussa, A.; Vaziri, S.; Fischer, A. C.; Sterner, M.; Forsberg, F.; Delin, A.; Esseni, D.; Palestri, P.; Ostling, M.; Lemme, M. C. Electromechanical Piezoresistive Sensing in Suspended Graphene Membranes. *Nano Lett.* **2013**, *13*, 3237−3242.

(9) Yuan, W.; Shi, G. Graphene-based Gas Sensors. *J. Mater. Chem. A* **2013**, *1*, 10078.

(10) Garaj, S.; Hubbard, W.; Reina, A.; Kong, J.; Branton, D.; Golovchenko, J. A. Graphene as a Subnanometre Trans-electrode Membrane. *Nature* **2010**, *467*, 190−193.

(11) Aleman, B.; Regan, W.; Aloni, S.; Altoe, V.; Alem, N.; Girit, C.; Geng, B.; Maserati, L.; Crommie, M.; Wang, F.; Zettl, A. Transfer-free Batch Fabrication of Large-area Suspended Graphene Membranes. *ACS Nano* **2010**, *4*, 4762−4768.

(12) Suk, J. W.; Kitt, A.; Magnuson, C. W.; Hao, Y.; Ahmed, S.; An, J.; Swan, A. K.; Goldberg, B. B.; Ruoff, R. S. Transfer of CVD-grown Monolayer Graphene onto Arbitrary Substrates. *ACS Nano* **2011**, *5*, 6916−6924.

(13) O'Hern, S. C.; Jang, D.; Bose, S.; Idrobo, J. C.; Song, Y.; Laoui, T.; Kong, J.; Karnik, R. Nanofiltration across Defect-Sealed Nanoporous Monolayer Graphene. *Nano Lett.* **2015**, *15*, 3254−3260.

(14) Martins, L. G.; Song, Y.; Zeng, T.; Dresselhaus, M. S.; Kong, J.; Araujo, P. T. Direct Transfer of Graphene onto Flexible Substrates. *Proc. Natl. Acad. Sci. U. S. A.* **2013**, *110*, 17762−17767.

(15) Sun, P.; Wang, K.; Zhu, H. Recent Developments in Graphene-Based Membranes: Structure, Mass-Transport Mechanism and Potential Applications. *Adv. Mater.* **2016**, *28*, 2287−2310.

(16) Novoselov, K. S.; Fal'ko, V. I.; Colombo, L.; Gellert, P. R.; Schwab, M. G.; Kim, K. A Roadmap for Graphene. *Nature* **2012**, *490*, 192−200.

(17) Strathmann, H.; Kock, K. The Formation Mechanism of Phase Inversion Membranes. *Desalination* **1977**, *21*, 241−255.

(18) Lehtinen, O.; Kotakoski, J.; Krasheninnikov, A. V.; Keinonen, J. Cutting and Controlled Modification of Graphene with Ion Beams. *Nanotechnology* **2011**, *22*, 175306.

(19) O'Hern, S. C.; Stewart, C. A.; Boutilier, M. S. H.; Idrobo, J. C.; Bhaviripudi, S.; Das, S. K.; Kong, J.; Laoui, T.; Atieh, M.; Karnik, R. Selective Molecular Transport through Intrinsic Defects in a Single Layer of CVD Graphene. *ACS Nano* **2012**, *6*, 10130−10138.

(20) Hu, S.; Lozada-Hidalgo, M.; Wang, F. C.; Mishchenko, A.; Schedin, F.; Nair, R. R.; Hill, E. W.; Boukhvalov, D. W.; Katsnelson, M. I.; Dryfe, R. A.; Grigorieva, I. V.; Wu, H. A.; Geim, A. K. Proton Transport through One-atom-thick Crystals. *Nature* **2014**, *516*, 227−230.

(21) Cohen-Tanugi, D.; Grossman, J. C. Water Permeability of Nanoporous Graphene at Realistic Pressures for Reverse Osmosis Desalination. *J. Chem. Phys.* **2014**, *141*, 074704.

(22) Xu, Z.-L.; Alsalhy Qusay, F. Polyethersulfone (PES) Hollow Fiber Ultrafiltration Membranes Prepared by PES/non-solvent/NMP solution. *J. Membr. Sci.* **2004**, *233*, 101−111.

(23) O'Hern, S. C.; Boutilier, M. S.; Idrobo, J. C.; Song, Y.; Kong, J.; Laoui, T.; Atieh, M.; Karnik, R. Selective Ionic Transport through Tunable Subnanometer Pores in Single-layer Graphene Membranes. *Nano Lett.* **2014**, *14*, 1234−1241.

(24) Rollings, R. C.; Kuan, A. T.; Golovchenko, J. A. Ion Selectivity of Graphene Nanopores. *Nat. Commun.* **2016**, *7*, 11408.

(25) Zou, X.; Zhang, L.; Wang, Z.; Luo, Y. Mechanisms of the Antimicrobial Activities of Graphene Materials. *J. Am. Chem. Soc.* **2016**, *138*, 2064−2077.

(26) Polsen, E. S.; McNerny, D. Q.; Viswanath, B.; Pattinson, S. W.; John Hart, A. High-speed Roll-to-roll Manufacturing of Graphene using a Concentric Tube CVD Reactor. *Sci. Rep.* **2015**, *5*, 10257.

DOI: 10.1021/acsami.7b00504
ACS Appl. Mater. Interfaces 2017, 9, 9239−9244

(27) Rahimpour, A.; Madaeni, S. S.; Mansourpanah, Y. High Performance Polyethersulfone UF Membrane for Manufacturing Spiral Wound Module: Preparation, Morphology, Performance, and Chemical Cleaning. *Polym. Adv. Technol.* **2007**, *18*, 403−410.
(28) Persson, K. M.; Capannelli, G.; Bottino, A.; Träg→dh, G. Porosity and Protein Adsorption of Four Polymeric Microfiltration Membranes. *J. Membr. Sci.* **1993**, *76*, 61−71.
(29) Jiang, D. E.; Cooper, V. R.; Dai, S. Porous Graphene as the Ultimate Membrane for Gas Separation. *Nano Lett.* **2009**, *9*, 4019−4024.
(30) Thiel, G. P. Salty Solutions. *Phys. Today* **2015**, *68*, 66−67.

DOI: 10.1021/acsami.7b00504
ACS Appl. Mater. Interfaces 2017, 9, 9239−9244